Title

Analysis of plasmaspheric hiss wave amplitudes inferred from low-altitude POES electron data: Validation with conjunctive Van Allen Probes observations

Authors

Soria-Santacruz, M
Li, W
Thorne, RM
et al.

Key Points:
- Determined the performance and limitations of the POES technique applied to hiss waves
- The POES technique performs well for moderate-to-strong hiss events at $L > 4$
- 97% of the inferred amplitudes are within a factor of 2.5 of the EMFISIS measurements

Correspondence to:
M. de Soria-Santacruz,
mariadesoria@gmail.com

Analysis of plasmaspheric hiss wave amplitudes inferred from low-altitude POES electron data: Validation with conjunctive Van Allen Probes observations

M. de Soria-Santacruz[1,2], W. Li[2], R. M. Thorne[2], Q. Ma[2], J. Bortnik[2], B. Ni[3], C. A. Kletzing[4], W. S. Kurth[4], and G. B. Hospodarsky[4]

[1]University Corporation for Atmospheric Research, Boulder, Colorado, USA, [2]Department of Atmospheric and Oceanic Sciences, UCLA, Los Angeles, California, USA, [3]Department of Space Physics, School of Electronic Information, Wuhan University, Wuhan, China, [4]Department of Physics and Astronomy, University of Iowa, Iowa City, Iowa, USA

Abstract Plasmaspheric hiss plays an important role in controlling the overall structure and dynamics of the Earth's radiation belts. The interaction of plasmaspheric hiss with radiation belt electrons is commonly evaluated using diffusion codes, which rely on statistical models of wave observations that may not accurately reproduce the instantaneous global wave distribution or the limited in situ satellite wave measurements. This paper evaluates the performance and limitations of a novel technique capable of inferring wave amplitudes from low-altitude electron flux observations from the Polar Orbiting Environmental Satellites (POES), which provide extensive coverage in L shell and magnetic local time (MLT). We found that, within its limitations, this technique could potentially be used to build a dynamic global model of the plasmaspheric hiss wave intensity. The technique is validated by analyzing the conjunctions between the POES spacecraft and the Van Allen Probes from September 2012 to June 2014. The technique performs well for moderate-to-strong hiss activity (≥ 30 pT) with sufficiently high electron fluxes. The main source of these limitations is the number of counts of energetic electrons measured by the POES spacecraft capable of resonating with hiss waves. For moderate-to-strong hiss events, the results show that the wave amplitudes from the EMFISIS instruments on board the Van Allen Probes are well reproduced by the POES technique, which provides more consistent estimates than the parameterized statistical hiss wave model based on CRRES data.

1. Introduction

The highly energetic particles of the Van Allen radiation belts pose a significant risk to satellites and astronauts in space [*Baker*, 2001], thus it is important to have predictive capability of the dynamic evolution of these regions. The energetic electron flux in the outer radiation belt can vary by several orders of magnitude in less than a day in response to solar activity. This variability is associated with an imbalance between source and loss processes which, in the case of electrons, is primarily caused by interactions with magnetospheric waves [*Xiao et al.*, 2009a, 2010; *Thorne*, 2010]. These waves are excited during magnetically active periods and lead to the violation of the particles' adiabatic invariants [*Schulz and Lanzerotti*, 1974]. Plasmaspheric hiss, which is an incoherent whistler mode emission found inside the dense plasmasphere and in dayside plasmaspheric plumes, is one of these waves. Hiss plays an important role in the dynamics of the magnetosphere, responsible for the formation of the slot region that appears between inner and outer radiation belts during quiet times [*Lyons and Thorne*, 1973; *Abel and Thorne*, 1998a]. It also contributes to the scattering of energetic outer belt electrons during active times [*Summers et al.*, 2008; *Ni et al.*, 2014a]. Moreover, pitch angle scattering by plasmaspheric hiss is also accredited with the slow decay of the electrons in the outer radiation belt following storm time enhancements [*Meredith et al.*, 2006, 2007, 2009; *Baker et al.*, 2007; *Xiao et al.*, 2009b; *Thorne et al.*, 2013]. It is crucial, therefore, to understand and predict the global dynamic evolution of the hiss power spectral intensity in the inner magnetosphere.

Current hiss wave models are based on statistics compiled from in situ satellite wave measurements in the inner magnetosphere. *Meredith et al.* [2004] was the first to put together a statistical model of the hiss wave intensity based on electric field data from the Combined Release and Radiation Effects Satellite (CRRES) and studied its dependence on substorm activity, magnetic local time (MLT), L shell, and latitude. Similarly,

Orlova et al. [2014] recently developed an empirical model of the plasmaspheric hiss intensity from CRRES observations and provided an analytical quadratic fit of the time-averaged magnetic field intensity as a function of K_p, L shell, latitude, and two MLT sectors. These wave models are commonly used in diffusion codes like the UCLA Full Diffusion Code [e.g., *Ni et al.*, 2008, 2011], which has been developed to evaluate the effects of the wave parameters on the dynamics of the radiation belts. Statistical models, however, may not reproduce the real, instantaneous global wave distribution. For this reason, reliable diffusion simulations capable of reproducing (and eventually predicting) the changes in the radiation environment are limited by the accuracy of the available global dynamic wave models.

In order to address this issue, the present paper uses a novel physics-based technique to calculate the hiss wave amplitude, which does not rely on in situ wave observations, but is instead based on low-altitude measurements of precipitating and trapped electrons from the Polar Orbiting Environmental Satellites (POES). POES are Sun-synchronous satellites at an altitude of ∼800 km with an orbital period of ∼100 min. Compared to the wave observations from other spacecraft, which are limited to a certain range in L shell and MLT, the multiple POES spacecraft provide extensive coverage thanks to their low-altitude polar orbit. The Medium Energy Proton and Electron Detector (MEPED) in the Space Environment Monitor (SEM-2) instrument package on board the POES spacecraft has two solid state particle telescopes capable of monitoring both energetic electrons and protons in different energy bands [*Evans and Greer*, 2004; *Green*, 2013]. The difference between the two telescopes is their orientation: the 0° pointing detectors have their field of view (±15° for both detectors) centered along the local zenith and pointing outward, while the 90° detectors are perpendicular to the former. Our technique uses the ratio between precipitating and trapped electron fluxes obtained from the MEPED instrument to infer the intensity of the hiss waves that produce such precipitation, which can well be described by quasi-linear theory [*Kennel and Petschek*, 1966]. *Ni et al.* [2014b] described this technique and the underlying physics in great detail, and *Li et al.* [2013a] used it to infer the global distribution of chorus waves. *Li et al.* [2013a] clearly showed that the correlation coefficient between measured and inferred wave power calculated from the ratio of trapped and precipitated fluxes is higher than that calculated using the individual fluxes alone, indicating that the use of this technique based on the ratio is better to estimate wave amplitudes. In a later paper, *Li et al.* [2014a] applied the methodology to hiss waves for a specific conjunction event between POES and the Van Allen Probes. More specifically, they used wave observations from the Electric and Magnetic Field Instrument and Integrated Science (EMFISIS) on board the Van Allen Probes (consisting of RBSP-A and RBSP-B) [*Kletzing et al.*, 2014] to validate the hiss wave intensity inferred from POES data. *Li et al.* [2014a] studied a moderately strong hiss event (>80 pT) and found that measured and calculated hiss wave amplitudes agreed within a factor of 2. In their paper, they already stated the key underlying assumptions and some of the limitations associated with applying the technique to hiss waves, which constitute the foundation of the present study. In this manuscript, we go one step farther and apply the technique to a number of conjunction events between POES and the Van Allen Probes from September 2012 to July 2014. The purpose of the study is to use the POES technique to infer the hiss wave amplitudes for these events and to determine its performance and limitations by comparing the results to conjunctive wave measurements from the Van Allen Probes. The performance is also assessed by comparing the inferred hiss wave amplitude using the POES technique to that of the CRRES statistical model from *Orlova et al.* [2014]; the dependence of the results on AL^* (minimum AL in the last 3 h), L shell, and MLT is also discussed. The sensitivity of the results to the input parameters of the technique is addressed in a separate study [*De Soria-Santacruz et al.*, 2015].

2. Methodology and Data Sets

POES data of energetic electron fluxes from the 0° and 90° telescopes are used to infer the equatorial hiss wave amplitude. Each detector has three integral energy channels: >30 keV, >100 keV, and >300 keV. Precipitating electron fluxes are measured by the 0° detector for $L > 1.4$ [*Rodger et al.*, 2010], while the 90° detector measures a mixture of particles in the drift and bounce loss cones as well as stably trapped particles over an invariant latitude between 55° and 68° [*Meredith et al.*, 2011]. The key element to the technique discussed in the present paper is the ratio between precipitating and trapped electron fluxes, which was described by *Li et al.* [2013a] and is repeated here for completeness.

$$C.R. \left(E_1 < E < E_2 \right)|_0 = \int_{E_1}^{E_2} \int_0^{2\pi} \int_0^{\beta} \frac{S(E)}{D_{\alpha\alpha}(E)|_{\alpha=\alpha_0} \cos\alpha_0} \frac{I_0 \left(\frac{\alpha_{eq,in}}{\alpha_0} z_0 \right)}{z_0 I_1(z_0)} A \sin\eta \, d\eta \, d\psi \, dE \qquad (1)$$

$$C.R. \left(E_1 < E < E_2\right)\big|_{90} = \int_{E_1}^{E_2} \int_{0}^{2\pi} \int_{0}^{\beta} \frac{S(E)}{D_{\alpha\alpha}(E)\big|_{\alpha=\alpha_0} \cos\alpha_0} \left[\frac{I_0(z_0)}{z_0 I_1(z_0)} + \ln\frac{\sin\alpha_{eq,out}}{\sin\alpha_0}\right] A \sin\eta \, d\eta \, d\psi \, dE \quad (2)$$

$$R = \frac{C.R. \left(E_1 < E < E_2\right)\big|_0}{C.R. \left(E_1 < E < E_2\right)\big|_{90}} \quad (3)$$

where $C.R.\big|_0$ and $C.R.\big|_{90}$ are the count rates measured by the 0° and 90° detectors on board the POES space-craft, respectively. E is the electron energy, E_1 and E_2 are the lower and upper electron energy bounds for the integration, $\beta = 15°$ is the field of view of the detector, A is the detector area, and η and ψ are related to the detector geometry and are represented in Figure 1b of *Li et al.* [2013a]. $S(E)$ is the electron energy spectrum, $D_{\alpha\alpha}(E)\big|_{\alpha=\alpha_0}$ is the pitch angle diffusion coefficient evaluated at the equatorial bounce loss cone α_0, $z_0 = \frac{2\alpha_0}{\sqrt{D_{\alpha\alpha}(E)\big|_{\alpha=\alpha_0} \cos\alpha_0 \tau_B}}$ where τ_B is the electron bounce period, I_0 and I_1 are modified Bessel functions of the first kind, and $\alpha_{eq,in}$ and $\alpha_{eq,out}$ are the equatorial pitch angle of the electrons inside and outside the loss cone, which can be expressed as a function of the detector geometry and orientation [*Ni et al.*, 2014b, equation (2)].

The pitch angle diffusion coefficient is a function of the plasma density, background magnetic field, and hiss wave normal distribution, normalized wave frequency spectrum (shape of the frequency spectrum), and amplitude. Therefore, for a given detector geometry, electron energy spectrum, magnetic field, plasma den-sity, and wave spectral properties, the equation above is solely a function of the hiss wave amplitude. In the present paper, we use analytical and statistical models to evaluate these input parameters. We purposely do not use direct observations of the input parameters because we attempt to evaluate the performance of this technique when in situ observations are not available; this would be the case if we want to build a global model of plasmaspheric hiss waves using POES data alone; thus, we would have to exclusively rely on mod-els of the input parameters. More specifically, we adopt the plasma density model given by *Sheeley et al.* [2001] inside the plasmasphere, a dipole model for the Earth's magnetic field, and a Kappa-type function with $\chi^2 = 0.05$ and $\kappa = 5$ to reproduce the shape of the electron energy spectrum [*Xiao et al.*, 2008; *Ni et al.*, 2014b]. The wave normal angle is considered Gaussian (field aligned at the equator and oblique at higher lat-itudes) with parameters given in Table 1 of *Ni et al.* [2013], while the normalized wave frequency spectrum is taken from a statistical model built from Van Allen Probes data. The statistical normalized hiss wave fre-quency spectrum is an input to the technique, and it was constructed under various levels of geomagnetic activity given by $AL^* \geq -100$ nT, -100 nT $> AL^* \geq -500$ nT, and $AL^* < -500$ nT, and for each individual con-junction event, we use the appropriate normalized frequency spectrum depending on the level of activity (we use AL because it is directly related to substorm activity). These inputs together with the precipitating and trapped electron flux data from the POES spacecraft and the UCLA Full Diffusion Code (used to calculate bounce-averaged diffusion coefficients using the expressions from *Glauert and Horne* [2005]), allow us to eval-uate equation (1) as a function of the magnetic wave amplitude for a broad range of L shells and MLT. It must be noted that most of the contributions to the bounce-averaged diffusion coefficient for $100-300$ keV elec-trons come from close-to-equatorial interactions because the minimum resonant energy rapidly increases with increasing latitude.

The purpose of this paper is to evaluate the performance and determine the limitations of the technique pre-sented above for plasmaspheric hiss. For this reason, the data set used in this study is built entirely out of conjunction events between the POES spacecraft and the Van Allen Probes. The hiss wave amplitudes inferred using the POES technique are compared to EMFISIS wave observations during conjunction events. EMFISIS provides routine measurements of all six electromagnetic components in the whistler mode band. The dif-ferent types of data from the EMFISIS instrument are presented in Figure 1, which were measured by RBSP-A on 23 May 2014. The AL index is shown in Figure 1a, which presents a major disturbance between 16:00 and 23:00 UT with values of $AL < -800$ nT; strong hiss waves (>50 pT) were generated during this geomagnetically active interval, which can be observed in the magnetic field spectral density of Figure 1b. Intense hiss waves are also observed earlier on that day, peaking below 1 kHz. It is interesting to note the very low frequencies covered by the hiss event at 16:00 UT, much lower than the standard ~550 Hz peak frequency commonly used in hiss wave models [e.g., *Lyons et al.*, 1972; *Abel and Thorne*, 1998a, 1998b; *Shprits et al.*, 2009; *Thorne et al.*, 2013; *Ni et al.*, 2013; *Orlova et al.*, 2014]. A similar low-frequency enhancement was already noted by *Li et al.* [2013b], which suggested that injected energetic electrons are responsible for the amplification of very low
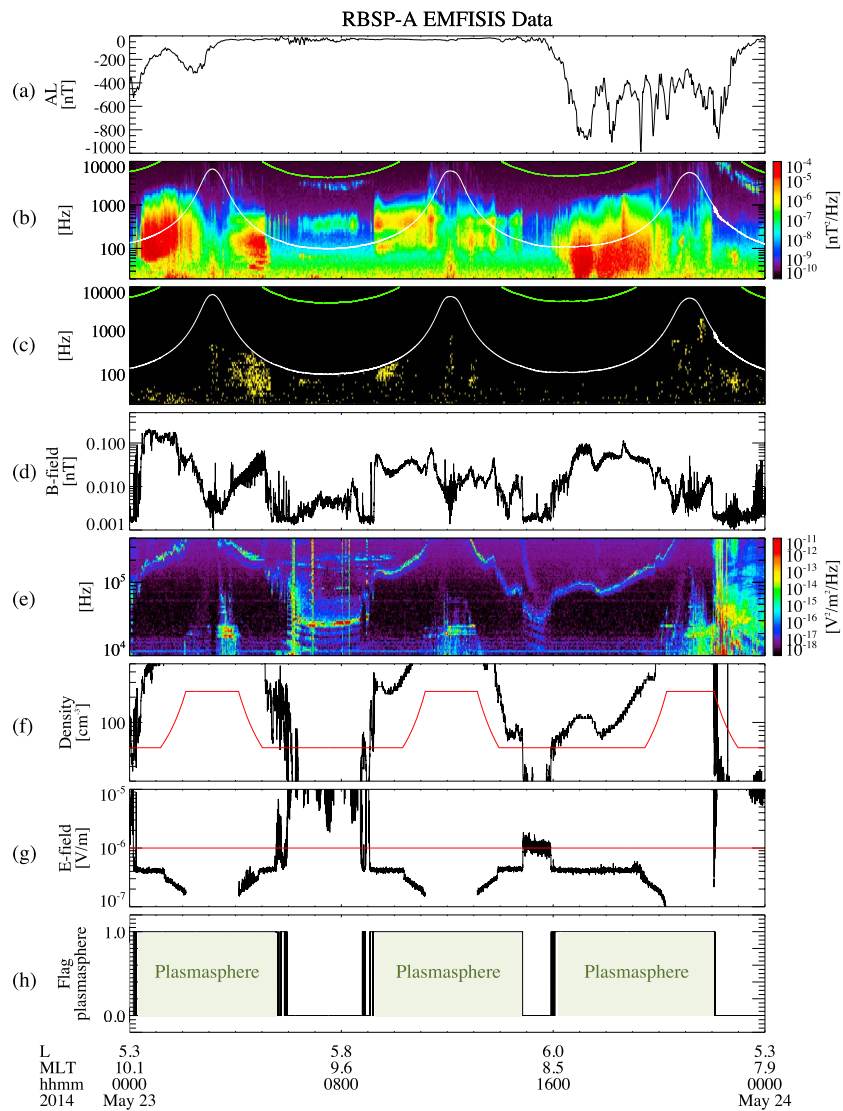
Figure 1. Van Allen Probe A observations during 23 May 2014. (a) *AL* index. (b) Frequency-time spectrogram of the magnetic field spectral density in the Waveform Receiver channel. (c) Flag indicating the presence of magnetosonic waves. Yellow (black) indicates the presence (absence) of magnetosonic wave power. The green and white lines in (b) and (c) are the electron cyclotron and lower hybrid frequencies, respectively. (d) Hiss magnetic wave amplitudes, excluding the contribution from magnetosonic waves. (e) Frequency-time spectrogram of the electric field spectral density in the HFR channel. (f) Density inferred from the upper-hybrid line (black) and density threshold used to determine the plasmaspheric region (red). (g) Electric field amplitude (black) and electric field threshold used to determine the plasmaspheric region (red). (h) Flag that indicates whether RBSP-A is inside (flag=1) or outside (flag=0) the plasmasphere.

frequency plasmaspheric hiss in the outer plasmasphere. This type of emissions are quite common [*Li et al.*, 2015] and need to be carefully discussed in future studies.

Equatorial magnetosonic waves need to be removed from the data set, which can have a similar frequency range to the lower frequency portions of hiss, in some spatial regions. Wave normal angle and wave polarization are used to identify magnetosonic waves, which are provided by EMFISIS Level 4 data. We have excluded those measurements with wave normal angle >80° and |ellipticity| < 0.2 inside the plasmasphere [*Horne et al.*, 2007], which are marked in yellow in Figure 1c and correspond to magnetosonic waves. The green and white lines in Figures 1b and 1c are the electron cyclotron and lower hybrid frequencies, respectively. The hiss magnetic field intensity is presented in Figure 1d, which is obtained by integrating the magnetic spectral intensity over frequencies between 50 Hz and 2000 Hz (but excluding the contribution of the magnetic
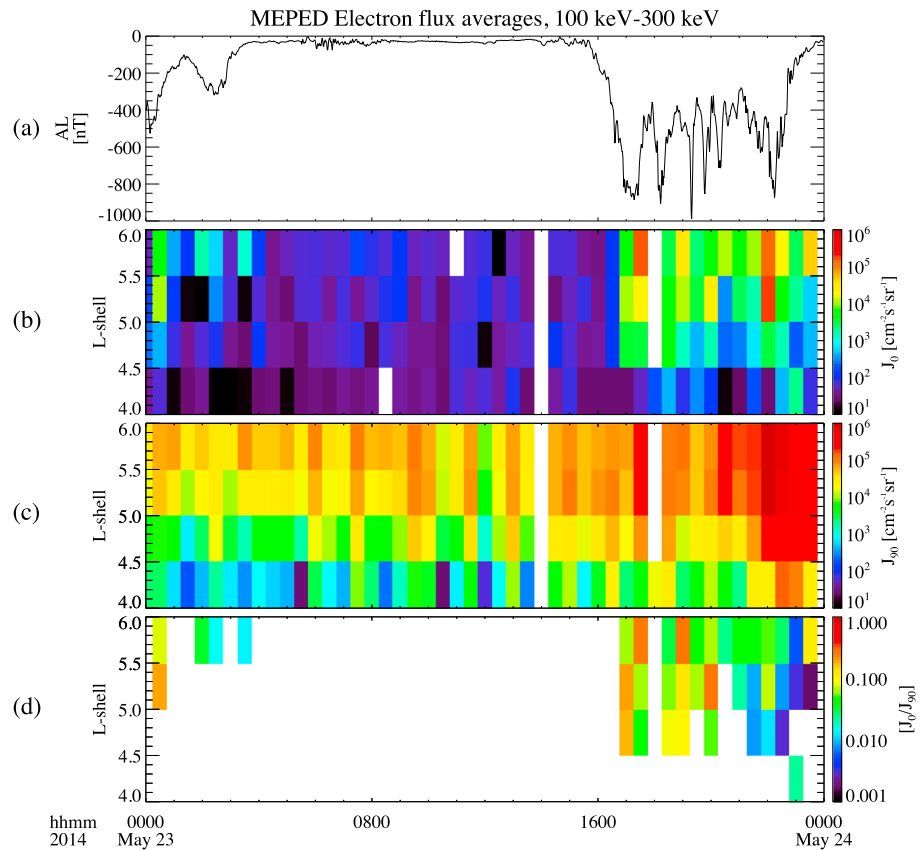
Figure 2. POES measurements of 100 keV to 300 keV electrons during 23 May 2014. (a) *AL* index. (b) J_0 is the flux measured by the 0° detector and (c) J_{90} is the flux measured by the 90° detector. (d) J_0/J_{90} averaged over bins of 0.5 *L* shell by 0.5 h (UT), over all POES spacecraft and over those MLTs corresponding to $L \geq 4$ of the RBSP-A orbit (MLT 06–12 in this case).

spectral intensity in the frequency bin corresponding to magnetosonic waves). In addition, chorus waves need to be excluded from the data set; thus, we only consider conjunction events with the Van Allen Probes inside the plasmasphere. More specifically, we use the inferred plasma density from the upper hybrid line and the electric field intensity measured by the High Frequency Receiver (HFR) to determine the location of the probes with respect to the plasmapause. The plasma density can be inferred from the upper hybrid line in the high flux reactor (HFR) spectra of Figure 1e. As an additional indicator of the plasmapause location, the electric field amplitude is obtained by integrating the HFR spectra over the electron cyclotron harmonic (ECH) frequency range based on the fact that ECH waves are much weaker inside the plasmapause, which is similar to the criteria used for the CRRES wave data analysis by *Meredith et al.* [2004]. The lower limit for integration of the HFR spectra corresponds to the minimum value between the electron cyclotron frequency and 10 kHz, while the upper limit equals 50 kHz. Plasma density and electric field are presented in Figures 1f and 1g, respectively. The plasma density inside the plasmasphere is required to be larger than a certain threshold, the latter shown in red in Figure 1f. This threshold is the maximum between 50 cm^{-3} and $n_{th} = (6.6/L)^4$ [*Li et al.*, 2010, equation (1)]. Similarly, the electric field inside the plasmasphere is required to be below 10^{-6} V/m, which is also plotted in red in Figure 1g. If one of these two criteria is not met, the measurement is considered outside the plasmasphere and it is excluded from the data set. Figure 1h presents a flag summarizing this analysis, which equals 1 when the satellite is inside the plasmasphere and 0 otherwise.

Figure 2 presents the fluxes measured by the POES spacecraft of 100–300 keV electrons, which have been obtained by subtracting the >300 keV electron channel from the >100 keV electron channel. The present study focuses on 100 keV to 300 keV electrons because they are shown to be more robust and reliable to infer the equatorial hiss wave intensity inside the plasmasphere (3 < *L* < 5) [*Meredith et al.*, 2004; *Li et al.*, 2014a]. The figure presents flux averages over bins of 0.5 *L* shell by 0.5 h (UT), over all POES spacecraft (METOP-A, NOAA-15, NOAA-16, NOAA-18, and NOAA-19), and over those MLTs corresponding to that portion of the RBSP-A orbit

with $L \geq 4$ (MLT 06–12 in this case). The proton contamination has been removed [*Lam et al.*, 2010] as well as those measurements inside the South Atlantic Anomaly. The precipitating electron flux measured by the 0° detectors is presented in Figure 2b. The POES technique does not perform well when the count rates are too low (e.g., below ∼5 counts/s, where the MEPED geometric factor of 100 cm^{-2} sr^{-1} is used to convert from fluxes to counts/s) since they get close to the background level. The applicability of the POES technique, therefore, has been limited to precipitating and trapped count rates >5 counts/s, which tend to occur in the outermost part of the plasmasphere at $L \geq 4$. Similarly, Figure 2c presents the flux measured by the 90° detectors. Both precipitating and trapped fluxes increased after the major AL disturbance at 16:00 UT. This enhancement is also shown in the ratio of precipitated to trapped fluxes of Figure 2d, which is only calculated for those bins with $J_0 \geq 500$ cm^{-2} s^{-1} sr^{-1} and is used to infer the wave amplitude from equation (1). While both precipitating and trapped electron fluxes are enhanced during geomagnetically active periods, it is only the ratio between precipitating and trapped electron fluxes that is positively correlated to the rate of diffusion through the formulation from *Kennel and Petschek* [1966].

3. Results and Validation of the Technique

The technique and inputs described above are used to infer the plasmaspheric hiss wave amplitudes during all the conjunction events between the POES spacecraft and the Van Allen Probes from 20 September 2012 to 30 June 2014. We define a conjunction event to be whenever a POES and an RBSP spacecraft meet in the same bin of dimensions 0.5 L shell by 0.5 h (UT) by 0.5 h (MLT), and for those intervals in which the RBSP spacecraft are inside the plasmasphere. The mapping between POES and RBSP is done using a dipole model for the Earth's magnetic field, since it works fairly well in the inner magnetosphere where plasmaspheric hiss is typically present. We note that the observations between POES and the Van Allen Probes may not be in perfect conjunction. However, inside the plasmasphere, the differences between various magnetic field models are insignificant during moderate-to-active geomagnetic conditions, as discussed in more detail below. Furthermore, our conjunction events represent "rough" conjunctions averaged over a bin size of 0.5 L shell by 0.5 h (UT) by 0.5 h (MLT) and hiss wave intensity does not change significantly in time and space within a comparable bin size; thus, a precise mapping is not essential in our study.

Only those conjunctions with observed $B_w \geq 30$ pT and observed fluxes $J_{0°}, J_{90°} \geq 500$ cm^{-2} s^{-1} sr^{-1} are considered. These constraints are not unique but have been selected based on obtaining a good performance (a factor of ∼2 or better between inferred and observed wave amplitudes) while still having a statistically relevant sample (74 conjunctions in this case). The precipitating electron fluxes driven by very weak waves (e.g., < 10 pT) appear to be similar due to the background contamination, and thus, the technique is not able to accurately calculate those small wave amplitudes; this is also the reason why we chose a modestly strong wave amplitude of 30 pT as a selection criterion. Inside the plasmasphere and for $L > 4$, the condition on the magnetic field (≥ 30 pT) is met 13% of the times based on Van Allen Probes wave data; if we additionally constrain the observations to those with $AL < -500$ nT, then the condition is met 25% of the times.

The 74 selected conjunctions are characterized in Figure 3, which presents histograms of these events as a function of L shell, MLT, and $AL*$. The different colors further classify the events by observed wave amplitude. It must be emphasized that the histograms in Figure 3 only show those events that satisfy the constraints described above (this is the 74 conjunctions). Therefore, the histograms are indicative of the distribution of the regions where the technique is valid. Figure 3a shows that most of the events occur between $L = 4$ and 5.5, and the most intense observations (> 120 pT) are localized in the L=4-4.5 bin. The MLT dependence in Figure 3b indicates that most of the hiss activity occurs on the dayside, between 06 and 18 MLT. Additionally, the hiss intensity on the nightside is substantially lower, which was already noted by *Meredith et al.* [2004] and *Li et al.* [2015]. Finally, Figure 3c shows that most of the events that satisfy the constraints imposed by the limitations of the technique ($B_w \geq 30$ pT and $J_{0°}, J_{90°} \geq 500$ cm^{-2} s^{-1} sr^{-1}) correspond to moderate-to-active geomagnetic conditions, and events with >90 pT are only observed during those conditions.

The performance of the POES technique is characterized in Figure 4. Figure 4a presents a scatterplot of the 74 conjunction events above, where the x axis corresponds to the hiss wave power observed by the Van Allen Probes (in pT^2) and the y axis shows the power inferred with the POES technique. If perfectly correlated, all the points would lie along the straight black dashed line. The correlation between the POES technique and the RBSP observations of Figure 4a (in green) is $C_{POES} = 0.46$, with 97% of the estimates being within a factor of 2.5 of the Van Allen Probes measurements. The constraints set on the technique, however, are not unique;
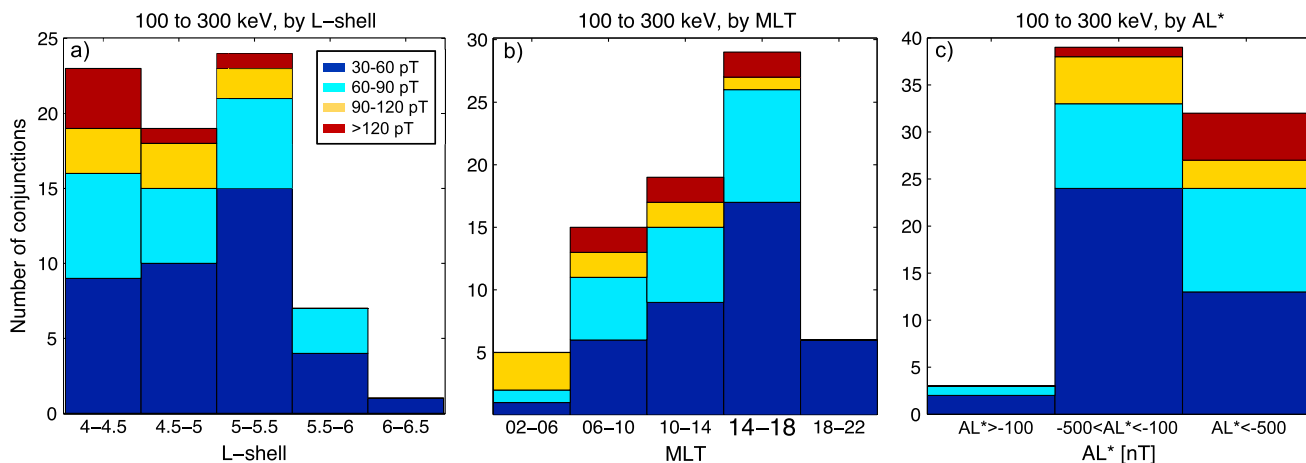
Figure 3. (a) *L* shell, (b) MLT, and (c) *AL** dependence of the conjunction events between the POES and the RBSP spacecraft from 20 September 2012 to 30 June 2014. The data set corresponds to events with observed wave amplitudes $\geq$ 30 pT and precipitating electron fluxes $\geq$ 500 cm^{-2} s^{-1} sr^{-1}. The events are also categorized in four levels of observed wave amplitude.

if we relax the constraint on the minimum observed wave amplitude to $B_w \geq 20$ pT (we get a new sample of 99 conjunctions), then the correlation decreases to $C_{POES} = 0.41$; if we decrease this constraint even further, the POES technique tends to overestimate the smaller wave amplitudes, which may be due to the larger obliqueness of these waves compared to the assumed wave normal angle distribution [*Li et al.*, 2014b] or to background contamination that requires larger POES fluxes to provide reliable results. Additionally, Figure 4a presents a comparison between the POES technique (in green) and the CRRES model of *Orlova et al.* [2014] (in red) for the same conjunction events (and therefore for the same geomagnetic conditions for each event). For each specific conjunction we have obtained the K_p and AL* measured during that epoch; K_p is an input to the CRRES parameterization, while AL* is used to determine the input-normalized frequency spectrum used by the POES technique. For each green event calculated with the POES technique there is a corresponding red event calculated with the statistical parameterization from Orlova et al. With a correlation of $C_{CRRES} = 0.37$, the plot reveals that the CRRES model consistently underestimates the wave amplitudes compared to RBSP measurements during the selected conjunctions. The origin of the underestimates given by the CRRES model may be due to two different factors: (1) the limited frequency coverage of the CRRES statistical model of hiss waves (>100 Hz) [*Meredith et al.*, 2004] and (2) the fact that the CRRES model is based on statistics categorized by geomagnetic activity levels where both weak and strong hiss could exist under a similar level of
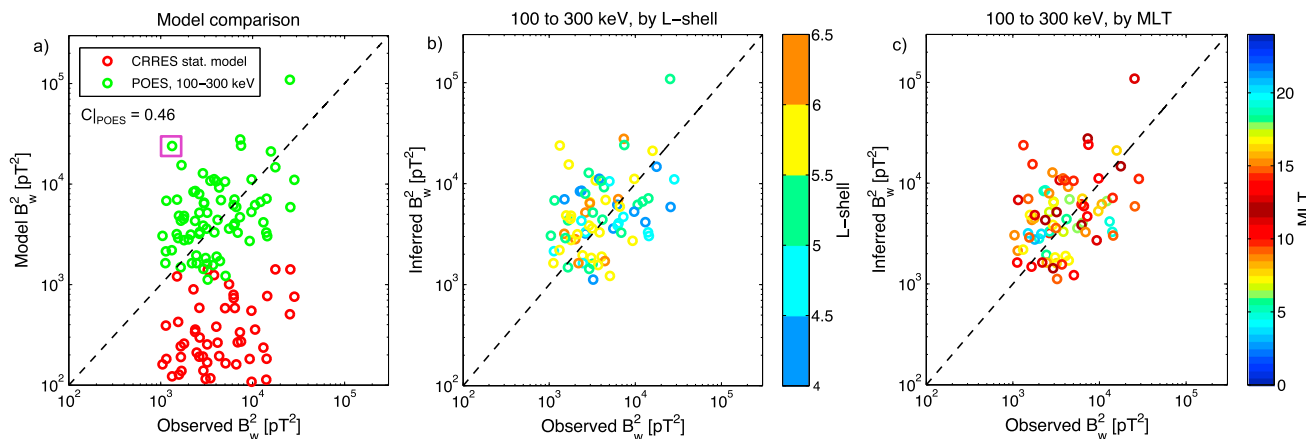
Figure 4. (a) Scatter plot of the calculated wave power (*y* axis) and the wave power observed by the Van Allen Probes (*x* axis) for the conjunction events in Figure 3a. The green markers have been calculated using the POES technique to infer the wave power, while the red markers correspond to the same conjunction events as the green ones but calculated using the Orlova et al. statistical parameterization of the hiss wave intensity. (b) *L* shell and (c) MLT dependence of the results from the POES technique in Figure 4a.
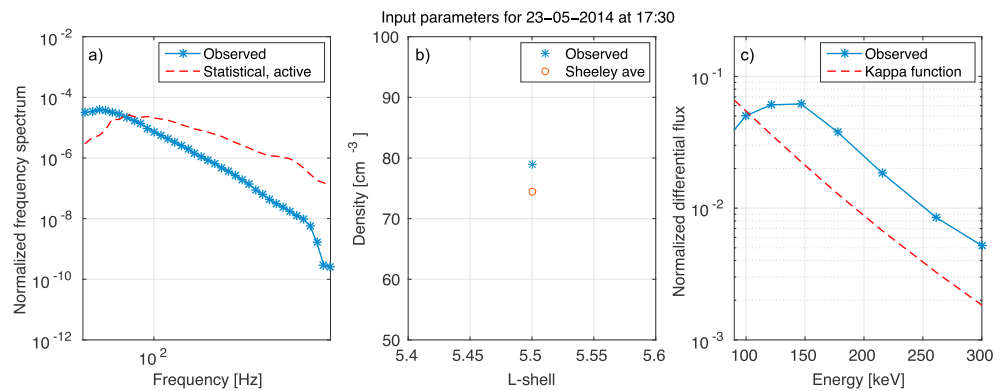
Figure 5. (a) Normalized frequency spectrum, (b) plasma density, and (c) electron energy spectrum corresponding to the hiss event observed by RBSP-A at 17:30 UT on 23 May 2014. The red dashed lines correspond to the input models used in the POES technique, while the solid blue lines are the values of the same parameters observed by RBSP-A.

geomagnetic activity, while our analysis using POES data only considers those events with moderate-to-strong hiss intensities $\geq$ 30 pT. Additionally, the color bars of Figures 4b and 4c show the dependence of the results from the POES technique (the green points in Figure 4a) on L shell and MLT, respectively. From Figure 4b we find that the performance of the technique does not seem to depend on L shell, that is, the most scattered points are not of any preferential color. Similarly, it is difficult to observe any trend with MLT in Figure 4c other than the fact that the sample mostly contains dayside events as described in Figure 3b. A similar analysis (not shown) was done to study the dependence on AL^*, which also showed that the performance of the technique does not follow any specific trend with this index.

We will focus now on the specific conjunction with observed $B_w^2 = 1326$ pT^2 and inferred $B_w^2 = 23880$ pT^2 enclosed in a purple box in Figure 4a, which corresponds to the worst performing event from the POES technique since the difference between modeled and observed wave amplitude is more than a factor of 4. The conjunction falls in the bin with $L = 5.5$, MLT= 9.5, and UT=17:30 on 23 May 2014 and between RBSP-A and METOP-02, which corresponds to the very low frequency event of Figure 1a and the precipitating fluxes of Figure 2. Which factor is primarily responsible for the misbehavior of the technique during this particular event? The problem could come from one of the input models used in the POES technique, that is, the models for the normalized frequency spectrum, density, and electron energy spectrum. A recent study on the topic by *De Soria-Santacruz et al.* [2015] shows that the POES technique is most sensitive to the shape of the input-normalized frequency spectrum, followed by the plasma density; the inferred wave amplitudes, however, are not very sensitive to the shape of the electron energy spectrum. As mentioned above, the results in Figure 4 used the density model from *Sheeley et al.* [2001], a statistical result of the hiss normalized frequency spectrum as a function of geomagnetic activity obtained from Van Allen Probes data, and a Kappa function representing the energy spectrum. For the conjunction selected above, Figure 5 compares the assumed inputs (red dashed lines) with their observed values (solid blue lines) obtained from in situ Van Allen Probes data averaged over the corresponding bin. Figure 5b shows that the Sheeley et al. model used in the technique reproduces reasonably well the density observed by the Van Allen Probes during this event. In Figures 5a and 5c we must emphasize that only the shape of the frequency and energy spectra matter to the technique and not their absolute value. In Figure 5a we find that the shape of the statistical normalized frequency spectrum peaks at higher frequencies and it is slightly flatter than the spectrum observed by the Van Allen Probes, which according to the results from *De Soria-Santacruz et al.* [2015] could be responsible for the deviation between inferred and observed wave amplitudes. The shape of the observed energy spectrum in Figure 5c is very similar to the Kappa function representation used in the POES technique except for energies below < 150 keV. Additionally, *De Soria-Santacruz et al.* [2015] showed that a Kappa function does a good job in inferring the wave amplitudes because the technique is not very sensitive to the electron energy spectrum. Detailed description of the sensitivity of the results to the inputs of the technique can be found in *De Soria-Santacruz et al.* [2015]. In spite of these issues, the technique performs well, that is, 97% of the estimates are within a factor of 2.5 of the observed wave amplitudes.

4. Discussion and Summary

In the sections above we used a novel technique to infer the plasmaspheric hiss wave amplitude from electron flux observations from the POES spacecraft. The main input to the methodology is the ratio between precipitating and trapped electron fluxes over $100-300$ keV, which depends on the rate of diffusion. The technique does not perform well at $L < 4$ because precipitating electron fluxes tend to be very low inside the slot region. If we know the wave amplitudes at higher L shells; however, it is possible to extend them to lower L shells using ray tracing and cyclotron/Landau damping techniques. The procedure of finding hiss wave amplitudes at low L shells (using ray tracing) from model results at higher L shells resembles the actual evolution that hiss experiences from their generation to their amplification, since chorus waves from outside the plasmasphere are believed to be a source for plasmaspheric hiss. *Bortnik et al.* [2008, 2009, 2011] and *Chen et al.* [2012a, 2012b] showed that chorus waves can leak through the plasmapause and evolve into hiss, the latter of which can undergo multiple reflections down to $L \approx 1.6$ before being Landau damped, thus filling the plasmasphere with the incoherent and structureless hiss.

The current paper evaluated the performance and limitations of the POES technique by analyzing all conjunction events between the Van Allen Probes and the POES spacecraft from 20 September 2012 to 30 June 2014. Only those events with observed wave amplitude ≥ 30 pT and precipitating electron fluxes ≥ 500 cm^{-2} s^{-1} sr^{-1} were considered, which correspond to events with moderate-to-strong hiss activity. These constraints are not unique but were selected to represent the limitations of the technique based on its performance. The results show that observed and inferred wave amplitudes agree reasonably well, that is, 97% of the estimates are within a factor of 2.5 of the Van Allen Probes measurements; the correlation coefficient between inferred and observed wave power is $C_{POES} = 0.46$. The relaxation of the constraint on the observed wave amplitude decreases the performance of the POES technique, which overestimates the smaller amplitudes; this behavior may be due to the larger obliqueness of these waves compared to the assumed wave normal angle distribution or to background contamination issues. Additionally, the performance of the technique does not seem to have a clear dependence on L shell, MLT, or AL^*. Moderate-to-strong hiss events (≥ 30 pT) occur mostly on the dayside and during moderate-to-active geomagnetic conditions; the difference in hiss intensity between dayside and nightside can be explained by the chorus origin of the hiss emissions since Landau damping is much stronger on the nightside compared to that on the dayside [e.g., *Bortnik et al.*, 2007].

The results of the hiss wave intensity from the POES technique were also compared with those from the statistical CRRES model of *Orlova et al.* [2014], the latter of which clearly underestimates the hiss wave amplitudes during the selected events. Since the Plasma Wave Experiment onboard the CRRES spacecraft only measured the electric field of the waves, we would expect that these measurements might lead to an overestimate of the magnetic field amplitude because the conversion from electric to magnetic fields involves the assumption of field-aligned waves. The persistent underestimation of hiss amplitudes by the CRRES statistical model must, therefore, be due to some other reason. One possible factor is that the CRRES model is based on averages categorized by geomagnetic activity levels where the hiss wave intensity could vary in an extensive range, while the conjunction events evaluated in this study are constrained to moderate-to-high amplitudes (≥ 30 pT). This is precisely the advantage of an event-specific versus a statistical model, since an event-specific model is capable of reproducing the instantaneous dynamic distribution of wave amplitudes. The second factor that could contribute to the underestimation is the frequency range of the CRRES instrument, which is limited to frequencies above 100 Hz. Plasmaspheric hiss, however, can peak at very low frequencies below 100 Hz, which is a common feature observed in the Van Allen Probes data. Moreover, the 15 month lifetime of CRRES was insufficient to provide extensive coverage over all L and MLT, particularly in the prenoon sector, which had poor coverage.

A particular conjunction for which the POES technique performed poorly was analyzed in more detail. We noted that the source of the discrepancy might be introduced by the inputs to the technique, which are the normalized frequency spectrum, density, and electron energy spectrum. The sensitivity of the technique to its inputs is analyzed in a separate paper [*De Soria-Santacruz et al.*, 2015].

In this paper we have validated the POES technique by determining its performance and limitations; we have shown that the methodology can provide instantaneous hiss wave amplitudes for moderate-to-strong hiss events within a factor of 2.5 of the Van Allen Probes measurements. The next step consists of investigating the possibility of building a plasmaspheric hiss model using POES particle measurements alone and for the specified limitations aided by the ray tracing simulation to estimate the hiss wave intensity further inside

the plasmasphere; the first step of the analysis would require gathering all the POES observations with high enough counts to satisfy the constraints detailed in this paper. Additionally, there are other challenges related to the exclusion of events associated with waves other than plasmaspheric hiss, that is, exclusion of precipitation introduced by chorus waves from POES data alone. We will then be able to exclude those intervals where the location of the POES spacecraft maps to regions outside the plasmasphere, therefore excluding chorus-driven precipitation from the data set.

References

Abel, B., and R. M. Thorne (1998a), Electron scattering loss in Earth's inner magnetosphere 1. Dominant physical processes, *J. Geophys. Res.*, *103*(A2), 2385–2396, doi:10.1029/97JA02919.

Abel, B., and R. M. Thorne (1998b), Electron scattering loss in Earth's inner magnetosphere: 2. Sensitivity to model parameters, *J. Geophys. Res.*, *103*(A2), 2397–2407, doi:10.1029/97JA02920.

Baker, D. N. (2001), Satellite anomalies due to space storms, in *Space Storms and Space Weather Hazards*, pp. 285–311, Springer, Netherlands.

Baker, D. N., S. G. Kanekal, R. B. Horne, N. P. Meredith, and S. A. Glauert (2007), Low-altitude measurements of 2–6 MeV electron trapping lifetimes at $1.5 \leq L \leq 2.5$, *Geophys. Res. Lett.*, *34*, L20110, doi:10.1029/2007GL031007.

Bortnik, J., R. M. Thorne, and N. P. Meredith (2007), Modeling the propagation characteristics of chorus using CRRES suprathermal electron fluxes, *J. Geophys. Res.*, *112*, A08204, doi:10.1029/2006JA012237.

Bortnik, J., R. M. Thorne, and N. P. Meredith (2008), The unexpected origin of plasmaspheric hiss from discrete chorus emissions, *Nature*, *452*(7183), 62–66, doi:10.1038/nature06741.

Bortnik, J., W. Li, R. M. Thorne, V. Angelopoulos, C. Cully, J. Bonnell, O. Le Contel, and A. Roux (2009), An observation linking the origin of plasmaspheric hiss to discrete chorus emissions, *Science*, *324*(5928), 775–778, doi:10.1126/science.1171273.

Bortnik, J., L. Chen, W. Li, R. M. Thorne, N. P. Meredith, and R. B. Horne (2011), Modeling the wave power distribution and characteristics of plasmaspheric hiss, *J. Geophys. Res.*, *116*, A12209, doi:10.1029/2011JA016862.

Chen, L., J. Bortnik, W. Li, R. M. Thorne, and R. B. Horne (2012a), Modeling the properties of plasmaspheric hiss: 1. Dependence on chorus wave emission, *J. Geophys. Res.*, *117*, A05201, doi:10.1029/2011JA017201.

Chen, L., J. Bortnik, W. Li, R. M. Thorne, and R. B. Horne (2012b), Modeling the properties of plasmaspheric hiss: 2. Dependence on the plasma density distribution, *J. Geophys. Res.*, *117*, A05202, doi:10.1029/2011JA017202.

De Soria-Santacruz, M., et al. (2015), Analysis of plasmaspheric hiss wave amplitudes inferred from low-altitude POES electron data: Technique sensitivity analysis, *J. Geophys. Res. Space Physics*, *120*, 552–3563, doi:10.1002/2014JA020865.

Evans, D. S., and M. S. Greer, (2004), Polar orbiting environmental satellite space environment monitor - 2: Instrument descriptions and archive data documentation, *Tech. Rep. 93, NOAA Tech. Mem.*, Space Weather Predict Cent., Boulder, Colo.

Glauert, S. A., and R. B. Horne (2005), Calculation of pitch angle and energy diffusion coefficients with the PADIE code, *J. Geophys. Res.*, *110*, A04206, doi:10.1029/2004JA010851.

Green, J. C. (2013), *MEPED Telescope Data Processing Algorithm Theoretical Basis Document*, Natl. Oceanic and Atmos. Admin. Space Environ. Cent., Boulder, Colo.

Horne, R. B., R. M. Thorne, S. A. Glauert, N. P. Meredith, D. Pokhotelov, and O. Santolík (2007), Electron acceleration in the Van Allen radiation belts by fast magnetosonic waves, *Geophys. Res. Lett.*, *34*, L17107, doi:10.1029/2007GL030267.

Kennel, C. F., and H. E. Petschek (1966), Limit on stably trapped particle fluxes, *J. Geophys. Res.*, *71*(1), 1–28.

Kletzing, C. A., et al. (2014), The Electric And Magnetic Field Instrument Suite And Integrated Science (EMFISIS) on RBSP, in *The Van Allen Probes Mission*, pp. 127–181, Springer, Netherlands.

Lam, M. M., R. B. Horne, N. P. Meredith, S. A. Glauert, T. Moffat-Griffin, and J. C. Green (2010), Origin of energetic electron precipitation >30 keV into the atmosphere, *J. Geophys. Res.*, *115*, A00F08, doi:10.1029/2009JA014619.

Li, W., R. M. Thorne, J. Bortnik, Y. Nishimura, V. Angelopoulos, L. Chen, J. P. McFadden, and J. W. Bonnell (2010), Global distributions of suprathermal electrons observed on THEMIS and potential mechanisms for access into the plasmasphere, *J. Geophys. Res.*, *115*, A00J10, doi:10.1029/2010JA015687.

Li, W., B. Ni, R. M. Thorne, J. Bortnik, J. C. Green, C. A. Kletzing, W. S. Kurth, and G. B. Hospodarsky (2013a), Constructing the global distribution of chorus wave intensity using measurements of electrons by the POES satellites and waves by the Van Allen Probes, *Geophys. Res. Lett.*, *40*, 4526–4532, doi:10.1002/grl.50920.

Li, W., et al. (2013b), An unusual enhancement of low-frequency plasmaspheric hiss in the outer plasmasphere associated with substorm-injected electrons, *Geophys. Res. Lett.*, *40*, 3798–3803, doi:10.1002/grl.50787.

Li, W., et al. (2014a), Quantifying hiss-driven energetic electron precipitation: A detailed conjunction event analysis, *Geophys. Res. Lett.*, *41*, 1085–1092, doi:10.1002/2013GL059132.

Li, W., et al. (2014b), Evidence of stronger pitch angle scattering loss caused by oblique whistler-mode waves as compared with quasi-parallel waves, *Geophys. Res. Lett.*, *41*, 6063–6070, doi:10.1002/2014GL061260.

Li, W., Q. Ma, R. M. Thorne, J. Bortnik, C. A. Kletzing, W. S. Kurth, G. B. Hospodarsky, and Y. Nishimura (2015), Statistical properties of plasmaspheric hiss derived from Van Allen Probes data and their effects on radiation belt electron dynamics, *J. Geophys. Res. Space Physics*, *120*, 3393–3405, doi:10.1002/2015JA021048.

Lyons, L. R., and R. M. Thorne (1973), Equilibrium structure of radiation belt electrons, *J. Geophys. Res.*, *78*(13), 2142–2149, doi:10.1029/JA078i013p02142.

Lyons, L. R., R. M. Thorne, and C. F. Kennel (1972), Pitch-angle diffusion of radiation belt electrons within the plasmasphere, *J. Geophys. Res.*, *77*(19), 3455–3474, doi:10.1029/JA077i019p03455.

Meredith, N. P., R. B. Horne, R. M. Thorne, D. Summers, and R. R. Anderson (2004), Substorm dependence of plasmaspheric hiss, *J. Geophys. Res.*, *109*, A06209, doi:10.1029/2004JA010387.

Meredith, N. P., R. B. Horne, S. A. Glauert, R. M. Thorne, D. Summers, J. M. Albert, and R. R. Anderson (2006), Energetic outer zone electron loss timescales during low geomagnetic activity, *J. Geophys. Res.*, *111*, A05212, doi:10.1029/2005JA011516.

Meredith, N. P., R. B. Horne, S. A. Glauert, and R. R. Anderson (2007), Slot region electron loss timescales due to plasmaspheric hiss and lightning-generated whistlers, *J. Geophys. Res.*, *112*, A08214, doi:10.1029/2007JA012413.

Meredith, N. P., R. B. Horne, S. A. Glauert, D. N. Baker, S. G. Kanekal, and J. M. Albert (2009), Relativistic electron loss timescales in the slot region, *J. Geophys. Res.*, *114*, A03222, doi:10.1029/2008JA013889.

Meredith, N. P., R. B. Horne, M. M. Lam, M. H. Denton, J. E. Borovsky, and J. C. Green (2011), Energetic electron precipitation during high-speed solar wind stream driven storms, *J. Geophys. Res.*, *116*, A05223, doi:10.1029/2010JA016293.

Ni, B., R. M. Thorne, Y. Y. Shprits, and J. Bortnik (2008), Resonant scattering of plasma sheet electrons by whistler-mode chorus: Contribution to diffuse auroral precipitation, *Geophys. Res. Lett.*, *35*, L11106, doi:10.1029/2008GL034032.

Ni, B., R. M. Thorne, N. P. Meredith, R. B. Horne, and Y. Y. Shprits (2011), Resonant scattering of plasma sheet electrons leading to diffuse auroral precipitation: 2. Evaluation for whistler mode chorus waves, *J. Geophys. Res.*, *116*, A04219, doi:10.1029/2010JA016233.

Ni, B., J. Bortnik, R. M. Thorne, Q. Ma, and L. Chen (2013), Resonant scattering and resultant pitch angle evolution of relativistic electrons by plasmaspheric hiss, *J. Geophys. Res. Space Physics*, *118*, 7740–7751, doi:10.1002/2013JA019260.

Ni, B., et al. (2014a), Resonant scattering of energetic electrons by unusual low-frequency hiss, *Geophys. Res. Lett.*, *41*, 1854–1861, doi:10.1002/2014GRL059389.

Ni, B., W. Li, R. M. Thorne, J. Bortnik, J. C. Green, C. A. Kletzing, W. S. Kurth, G. B. Hospodarsky, and M. Soria-Santacruz Pich (2014b), A novel technique to construct the global distribution of whistler mode chorus wave intensity using low-altitude POES electron data, *J. Geophys. Res. Space Physics*, *119*, 5685–5699, doi:10.1002/2014JA019935.

Orlova, K., M. Spasojevic, and Y. Shprits (2014), Activity-dependent global model of electron loss inside the plasmasphere, *Geophys. Res. Lett.*, *41*, 3744–3751, doi:10.1002/2014GL060100.

Rodger, C. J., M. A. Clilverd, J. C. Green, and M. M. Lam (2010), Use of POES SEM-2 observations to examine radiation belt dynamics and energetic electron precipitation into the atmosphere, *J. Geophys. Res.*, *115*, A04202, doi:10.1029/2008JA014023.

Schulz, M., and L. J. Lanzerotti (1974), *Particle Diffusion in the Radiation Belts*, Springer, New York.

Sheeley, B. W., M. B. Moldwin, H. K. Rassoul, and R. R. Anderson (2001), An empirical plasmasphere and trough density model: CRRES observations, *J. Geophys. Res.*, *106*(A11), 25,631–25,641.

Shprits, Y. Y., D. Subbotin, and B. Ni (2009), Evolution of electron fluxes in the outer radiation belt computed with the verb code, *J. Geophys. Res.*, *114*, A11209, doi:10.1029/2008JA013784.

Summers, D., B. Ni, N. P. Meredith, R. B. Horne, R. M. Thorne, M. B. Moldwin, and R. R. Anderson (2008), Electron scattering by whistler-mode elf hiss in plasmaspheric plumes, *J. Geophys. Res.*, *113*, A04219, doi:10.1029/2007JA012678.

Thorne, R. M. (2010), Radiation belt dynamics: The importance of wave-particle interactions, *Geophys. Res. Lett.*, *37*, L22107, doi:10.1029/2010GL044990.

Thorne, R. M., et al. (2013), Evolution and slow decay of an unusual narrow ring of relativistic electrons near $L \sim 3.2$ following the September 2012 magnetic storm, *Geophys. Res. Lett.*, *40*, 3507–3511, doi:10.1002/grl.50627.

Xiao, F., C. Shen, Y. Wang, H. Zheng, and S. Wang (2008), Energetic electron distributions fitted with a relativistic Kappa-type function at geosynchronous orbit, *J. Geophys. Res.*, *113*, A05203, doi:10.1029/2007JA012903.

Xiao, F., Z. Su, H. Zheng, and S. Wang (2009a), Modeling of outer radiation belt electrons by multidimensional diffusion process, *J. Geophys. Res.*, *114*, A03201, doi:10.1029/2008JA013580.

Xiao, F., Q. Zong, and L. Chen (2009b), Pitch-angle distribution evolution of energetic electrons in the inner radiation belt and slot region during the 2003 Halloween storm, *J. Geophys. Res.*, *114*, A01215, doi:10.1029/2008JA013068.

Xiao, F., Z. Su, H. Zheng, and S. Wang (2010), Three-dimensional simulations of outer radiation belt electron dynamics including cross-diffusion terms, *J. Geophys. Res.*, *115*, A05216, doi:10.1029/2009JA014541.